Energy Conversion and Management 196 (2019) 807–820

Contents lists available at ScienceDirect

Energy Conversion and Management

journal homepage: www.elsevier.com/locate/enconman

Simplified heat transfer model for parabolic trough solar collectors using supercritical CO_2

Rafael Aguilar[a], Loreto Valenzuela[a,*], Antonio L. Avila-Marin[a], Pedro L. Garcia-Ybarra[b]

[a] CIEMAT, Plataforma Solar de Almería, Crta. de Senés, km. 4.5, E04200 Tabernas, Almería, Spain
[b] UNED, Dept. Física Matemática y Fluidos, Senda del Rey 9, E28040 Madrid, Spain

ARTICLE INFO

Keywords:
Solar energy
Parabolic-trough collector
Receiver tube
Heat transfer model
Supercritical carbon dioxide

ABSTRACT

The main Concentrated Solar Power (CSP) plants type installed worldwide corresponds to parabolic trough (PT) technology transforming solar energy into thermal energy on the receiver tubes. The use of alternative Heat Transfer Fluids (HTF) in order to increase the solar-to-electric efficiency by means of either higher HTF temperatures or the use of supercritical cycles have opened a new line of research. In this framework, super-critical carbon dioxide (sCO_2) seems to be a good candidate to replace current HTFs in PTs. This work implements a one-dimensional heat transfer model for a PT solar collector considering different HTFs such as synthetic oil, sub-critical carbon dioxide, and sCO_2. The numerical results of the outlet fluid temperature are compared to experimental data and numerical results published in the literature, obtaining maximum temperature deviations of 0.9%, 2.9% and 2.7% respectively. Finally, a sensitivity analysis was conducted to evaluate the influence of the solar irradiation, mass flow rate and HTF inlet temperature on the thermal performance of a PT working with sCO_2 showing that the solar irradiation produces the greatest variations.

1. Introduction

Energy production is undoubtedly one of the challenges facing present-day society. The increasing energy demand, the harmful effects caused by greenhouse gases, as well as the depletion of fossil fuel resources, makes the current energy mix environmentally unsustainable [1]. Such environmental energy issues have fostered the development of renewables energies in general and Concentrated Solar Power (CSP) technologies in particular. Among all solar thermal technologies, Parabolic Trough Collector (PTC) is the most commercially deployed technology [2,3], however the electricity cost is still not competitive with fossil fuels. So, in order to increase PTC solar-to-electric efficiency and reduce its costs, several research initiatives are in progress [4].

Increasing the outlet Heat Transfer Fluid (HTF) temperatures are currently pursued to increase the PTC thermal-to-electric efficiency. On the one hand, increasing the temperature increases the PTC thermal losses, but on the other hand, it increases the power cycle efficiency [5]. It is demonstrated that each concentration factor presents a temperature at which the thermal-to-electric efficiency gets a maximum.

Nowadays, one of the main constraints of PTC facilities comes from the HTFs [6], because the most widely used commercial fluid in PTC plants is biphenyl/diphenyl oxide synthetic oil that is rapidly degraded if 400 °C is exceeded, conditioning its performance by delimitation of the operation range temperature [7].

The use of alternative HTFs that are not temperature limited is a must [8], and pressurized gases enable to reduce the difficulties related to actual HTFs. Besides that, the wider operational temperature range increases the overall plant performance. Recently, carbon dioxide (CO_2) has been considered an alternative to conventional HTF in PTC [9], which have been used for cooling applications of nuclear reactors since 1970 [10]. A remarkable aspect of CO_2 is that its critical state is easily reached with PTC systems [11]. Specifically, it behaves like a supercritical fluid above its critical temperature (304.13 K) and critical pressure (7.38 MPa) adopting properties half-way between a gas and a liquid. Supercritical state provides to CO_2 (sCO_2) advantages for reaching higher efficiencies in super-critical cycles [12] at relatively low temperatures, since it can be used in the receiver and the gas turbines at same time removing heat exchanger for energy production [13]. The potential of sCO_2 as HTF explains the growing interest in the development and design of suitable components for commercial

Abbreviations: CIEMAT, Centro de Investigaciones Energéticas Medioambientales y Tecnológicas; CSP, Concentrated solar power; HCE, Heat collector element; HTF, Heat transfer fluid; IAM, Incidence angle modifier; IFL, Innovative Fluids Loop; OAT, One-at-a-time; PSA, Plataforma Solar de Almería; PT, Parabolic-trough; PTC, Parabolic-trough collector; SNL, Sandia National Laboratories; STE, Solar thermal electricity; 1-D, One-dimensional; 2-D, Two-dimensional

* Corresponding author.
E-mail address: loreto.valenzuela@psa.es (L. Valenzuela).

https://doi.org/10.1016/j.enconman.2019.06.029
Received 29 March 2019; Received in revised form 23 May 2019; Accepted 14 June 2019

Nomenclature

A	Cylinder lateral area, m^2
b	Interaction coefficient, dimensionless
c_p	Specific heat capacity, J/(kg·K)
D	Diameter, m
D	Deviation, %
G_b	Direct solar irradiance, W/m^2
f_2	Darcy friction factor, dimensionless
f_c	Focal distance, m
h	Convection heat transfer coefficient, $W/(m^2·K)$
k	Thermal conductivity, W/(m·K)
$K(\theta)$	Incident angle modifier, dimensionless
L	Total receiver length, m
$\dot{m}$	Mass flow, kg/s
N	Number of nodes, dimensionless
Nu	Nusselt number, dimensionless
Pr	Prandtl number, dimensionless
r	Mirrors reflectance, dimensionless
Ra	Rayleigh number, dimensionless
Re	Reynolds number, dimensionless
T	Temperature, K
w	Aperture length of the collector, m

Greek symbols

α	Absorptivity, dimensionless
δ	Thickness, m
γ_C	Intercept factor of the solar concentrator, dimensionless
γ_R	Effective length factor of the receiver tubes, dimensionless
γ_T	Overall intercept factor, dimensionless
ε	Emissivity, dimensionless
λ	Mean-free-path between collisions of a molecule, m
$\eta_{opt,0^\circ}$	Nominal optical efficiency, dimensionless
η	Thermal efficiency, dimensionless
μ	Dynamic viscosity, kg/(m·s)
σ	Stefan-Boltzmann constant, $5.67{\cdot}10^{-8} W/(m^2·K^4)$
τ	Transmittance, dimensionless
θ	Angle of incidence of the beam solar radiation, degrees

Subscripts

a	Absorber tube
amb	Ambient
conv	Convection
f	Fluid
g	Glass cover
i	Inner
o	Outer
rad	Radiation
T	Temperature
v	Vacuum

Superscripts

exp	Experimental
i	Inlet of the receiver tube
num	Numerical
o	Outlet of the receiver tube

applications [14]. A detailed literature review of sCO_2 Brayton cycles in a wide variety of power generation applications has been performed by Manjunath et al. [15].

The heat transfer characteristics of PTC are essential to evaluate the thermal losses and improve its thermal performance, and they have received much attention in the literature. Briefly, the main works dealing with the thermal analysis of PTCs are presented. Forristall [16] carried out a detailed numerical heat transfer analysis of PTC, implemented in Equation Engineering Solver (EES), validated with experimental data from Sandia National Laboratories (SNL), using thermal oil as HTF. Dudley et al. [17] developed an analytical one dimensional (1-D) steady state model of a LS-2 parabolic solar collector under three different receiver configurations and two different selective absorbing coatings validated with experimental data collected by SNL. Gong et al. [18] presented an optimized model, programmed in Matlab that was compared with tests performed in the first high temperature PTCs, in China. A detailed radiative heat transfer analysis and more accurate heat transfer correlations were proposed by Padilla et al. [19] showing good agreement with experimental data, and in comparison with other heat transfer models. Kalogirou et al. [20] considered conduction through the absorber pipe and glass cover simultaneously, modelled in EES, and validated with data of existing collectors. A new numerical thermal model for Direct Steam Generation (DSG) in PTC with non-uniform heat flux implemented in Matlab was developed by Serrano-Aguilera et al. [21] evaluating thermal gradients in the absorber wall, and glass envelope. Qiu et al. [22] develop a detailed three-dimensional model combining Monte Carlo ray tracing and finite volume method to investigate the thermal performance of a PTC using sCO_2 as the HTF under two typical conditions for the sCO_2 Brayton and Rankine cycles.

This work presents a simplified 1-D model for a PTC to be used for different operating conditions and HTFs, focusing in sCO_2 in an attempt to provide knowledge about the thermal performance with PTC. Firstly, the implemented thermal model is used for state-of-the-art silicone thermal oil, and carbon dioxide at subcritical state and the numerical results are compared with experimental tests from Plataforma Solar de Almería (PSA), Spain. Secondly, the sCO_2 is considered as HTF in the 1-D model and the numerical results are compared with numerical literature data, as there are not available experimental results. Finally, a sensitivity analysis for sCO_2 has been carried out to analyse the influence of the main operational PTC parameters, solar irradiation, mass flow rate and HTF inlet temperature, on the outlet fluid temperature in order to asses operational conditions.

2. Methodology

2.1. Solar receiver description

A PTC consists of a parabolic reflector with solar tracking that reflects the direct solar radiation concentrating it on a linear receiver placed in the focus of the parabola, heating up the fluid that flows through, transforming the solar radiation into thermal energy. These collectors use support structures to conform the reflecting surface. In order to compare the numerical results obtained in this work with experimental values published previously, two collector designs have been considered: URSSATrough for thermal oil and EuroTrough for carbon dioxide [23].

Firstly, the solar collector tested was the URSSATrough collector, manufactured by the Spanish company URSSA Energy Corporation. The prototype installed at the HTF test loop of the PSA is composed of 18 receiver tubes with a total length of 75 m, 28 reflectors facets per module, ball joints at the inlet and flexible hose plus swivel joint at the outlet. It was placed in an East-West orientation and the tracker is based in sun position algorithm [24]. The main parameters of the collector installed at PSA are presented in Table 1.

Secondly, a EuroTrough-type module was examined in order to

Table 1
URSSATrough parabolic-trough collector characteristics.

Parameter	Value	Unit
Number of modules	6	–
Receiver tubes per module	3	–
Collector length(L)	75	m
Aperture of the collector(w)	5.76	m
Focal distance(f_c)	1.71	m
Mirrors solar reflectance(r)	0.93	–
Effective length factor(γ_R)	0.960	–
Solar intercept factor(γ_C)	0.958	–
Overall intercept factor(γ_T)	0.920	–
Nominal optical efficiency $\left(\eta_{opt,0^\circ}\right)$	0.78	–
Incident angle modifier($K(\theta)$)	$K(\theta) = 1 - \frac{(7\cdot10^{-4})\cdot\theta - (36\cdot10^{-6})\cdot\theta^2}{\cos(\theta)}$	–

Fig. 1. View of the pressurised gas test loop with PTCs at PSA.

Table 2
EuroTrough ET-50 parabolic-trough collector characteristics.

Parameter	Value	Unit
Number of modules	4	–
Receiver tubes per module	3	–
Collector length(L)	50	m
Aperture of the collector (w)	5.76	m
Focal distance(f_c)	1.71	m
Mirrors solar reflectance(r)	0.93	–
Effective length factor(γ_R)	0.960	–
Solar intercept factor(γ_C)	0.958	–
Overall intercept factor(γ_T)	0.920	–
Nominal optical efficiency $\left(\eta_{opt,0^\circ}\right)$	0.78	–
Incident angle modifier($K(\theta)$)	$K(\theta) = 1 - \frac{(1.88\cdot10^{-3})\cdot\theta - (1.492\cdot10^{-4})\cdot\theta^2}{\cos(\theta)}$	–

present results for a realistic collector in the temperature range of 200–400 °C in the attempt to achieve a more competitive generation of solar energy based on expectations of lower cost and higher collector performance [25]. The experimental Innovative Fluids Loop (IFL) plant, sited at PSA, consists of two collectors placed in an East-West orientation with a length of 50 m each and operated in series (Fig. 1). This test loop was designed to work at pressures and temperatures of up to 100 bar and 500 °C. The facility is completed with a blower that supplies the necessary flow to the gas, an air cooler used to dissipate the heat absorbed into the atmosphere and an auxiliary circuit that allows charging gases in the test loop. The objective of this installation is the study of pressurized gases as HTFs in PTCs, evaluating their behaviour under different real operating conditions. The main parameters of the EuroTrough collectors installed in the IFL plant are presented in Table 2.

The receiver of the PTC, named Heat Collector Element (HCE), consists of an absorber tube inside a glass envelope with expansion bellows at both ends. The absorber tube is made of stainless steel, alloy 321, with a selective coating on the outside surface to provide the suitable optical and radiative properties. This coating combines high absorptivity ($\alpha \sim 0.95$) in the solar radiation spectrum with a low emittance ($\varepsilon_{400^\circ C} \leq 0.15$) to the temperature range in which the surface emits radiation. The thermal energy absorbed by the HCE is transferred to the HTF.

The glass envelope protects the absorber tube. It is typically made in borosilicate glass, which maintains optimal strength and transmittance under high temperatures. The glass envelope is usually subjected to an anti-reflective coating to increase its transmissivity and, consequently, the optical performance of the collector ($\tau \sim 0.96$). The annulus space between the absorber and the glass envelope is under vacuum to reduce thermal losses. The vacuum also serves to protect the selective coating. The getter material disposed between the glass envelope and the absorber tube serves to remove hydrogen in the annulus space, assisting in maintaining the vacuum. The bellows provide a glass-to-metal seal and allow a thermal expansion between the metal absorber and glass envelope. The space between bellows offers a place to attach the HCE support brackets.

The receiver tube is nowadays widely spread in commercial CSP applications [8]. PTR®70 receivers, manufactured by the German company Schott [26], are installed in PTC as the HCEs and have been selected in this study. The main parameters are presented in Table 3.

2.2. Heat transfer fluids

A crucial decision in the design of a CSP plant is the choice of the HTF to be used, since the overall performance of the system highly depends on the fluid [6]. The working fluid used in the PTC depends on the purpose for which it is needed, that is, on the temperature to be achieved. There are several general criteria including physical and chemical properties, environmental and operational safeties, design and economy that the working fluid should ideally satisfy to be used [9]. Different HTFs have been used over the past years, however research continues to find out more efficient fluids.

This work has considered two HTFs to numerically analyse their thermal performance: thermal oil and carbon dioxide. The thermal oil Syltherm®800 was used to verify the validity of the implemented model

Table 3
Schott PTR®70 receiver technical specifications.

Parameter	HTF	Value	Unit
Receiver length(L)		4.06	m
Annular vacuum pressure		10^{-3}	mbar
Absorber tube outer diameter ($D_{a,o}$)		0.07	m
Absorber tube inner diameter($D_{a,i}$)	(Thermal oil)	0.066	m
Thickness of the absorber tube (δ_a)	(Thermal oil)	0.002	m
Absorber tube inner diameter ($D_{a,i}$)	(Carbon dioxide)	0.058	m
Thickness of the absorber tube (δ_a)	(Carbon dioxide)	0.006	m
Absorber tube inner roughness(e)		$6.8250\cdot10^{-06}$	m
Absorber tube emissivity@400 °C (ε_a)		0.095	–
Absorber tube absorptivity(α_a)		0.96	–
Glass envelope outer diameter ($D_{g,o}$)		0.125	m
Glass envelope inner diameter ($D_{g,i}$)		0.119	m
Thickness of glass envelope(δ_g)		0.003	m
Glass envelope emissivity (ε_g)		0.86	–
Glass envelope absorptivity(α_g)		0.02	–
Glass envelope transmittance(τ_g)		0.96	–

for its later use. This fluid has been widely used and it is commercially available, so it is not complicated to get real operation data to compare with the numerical results.

Supercritical carbon dioxide (sCO_2) has characteristics that make it a good choice as HTF, leading to a growing interest in its use for CSP technology [27]. Following this trend, carbon dioxide has been used at both subcritical and supercritical states in simulations. In the following sections, a brief review of the heat transfer fluids considered in the present work is presented.

2.2.1. Synthetic oil

Among the different types of synthetic thermal oils commercially available, Syltherm®800 is selected due to the availability of experimental data about its performance as working fluid in parabolic troughs. Syltherm®800 is a synthetic oil based on low viscosity silicones that offer excellent heat transfer performance. Among the synthetic oils is the one with the most extensive operational temperature, it is stable and durable in the range from −40 °C to 400 °C. The fluid is essentially odourless, low in acute oral toxicity and noncorrosive toward common metals and alloys [28].

Thermal oils have been used as HTFs because of their affordable price, low vapour pressure, good thermal stability, and long lifetime. However, they also have some important constraints; such as the temperature range, the high cost, and the necessity of heat exchangers to transfer thermal energy to the power cycle.

2.2.2. Carbon dioxide

The use of pressurized gases as HTFs on PTCs is an innovative idea to improve the overall performance of the system. As Muñoz-Antón et al describes in [29], CO_2 has advantageous properties compared to the different gas options investigated, so its use as HTF has been proposed for CSP technologies [30] to overcome the temperature restrictions and drawbacks found with thermal oil, molten salt, and steam [31]. CO_2 as working fluid have been applied in many fields, such as gas-cooled nuclear reactors, extraction solvent in food production or dry-cleaning for textile industry [32].

CO_2 is non-toxic, readily available, inexpensive, environmental friendly, non-flammable, stable at high temperature, with a large operational temperature range (-73 °C to 1000 °C) [33]. Moreover, it presents a critical state above 304.13 K and 7.38 MPa which are easily reached at PTC working conditions [9], and at these conditions it can be used directly in supercritical cycles [13].

A supercritical fluid is any substance at a temperature and pressure at/or above its critical point, where it can adopt properties mid-way between a gas and a liquid. The sCO_2 critical point is observed at the pressure of 73.8 bar and the temperature of 31 °C in the P-T diagram (Fig. 2). Supercritical conditions means that CO_2 expands to fill its container like a gas but with the density of a liquid performing like a single-phase fluid. Due to its high density, a relatively low fluid flow rate is required for sCO_2, which reduces significantly the compression work and lead to simpler and compactor turbines designs working at higher temperatures promising substantial improvements in system efficiency [34]. Moreover, the heat transfer coefficient of sCO_2, which is critical to lower the temperature difference between the metal tube and the fluid, especially because the non-uniform heat flux distribution on the outer surface of the metallic absorber tube, is greater than that of gases such as air or N_2 [35]. The NIST database is used to get the thermal properties for sCO_2 [36].

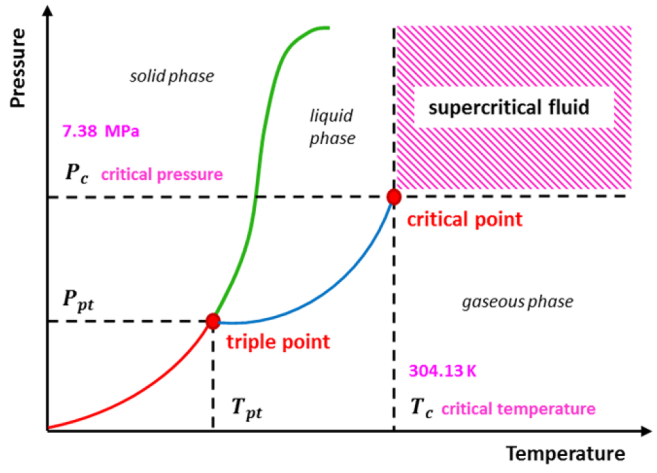

Fig. 2. P-T diagram phases to carbon dioxide.

sCO_2 can be used as both, HTF for the solar collector and as the working fluid for the power cycle. This eliminates the need of a heat exchanger which results in more efficient and less complex power units. Due to its thermodynamic properties, sCO_2 operated in a Brayton cycle provides higher temperature operability than steam, and has the potential of achieve higher efficiency than a helium-Brayton cycle at lower temperature ranges (Fig. 3) [37]. As a result, CO_2 at subcritical and supercritical conditions are considered as HTF in this study.

Despite sCO_2 benefits, it also presents some challenges that need to be addressed. Operating near the critical point means high working pressures, so reduced tube diameters are required leading in a reduction in the heat transfer rate in tubular receivers. As well as the possible leaks associated to moving parts and connections. Accordingly the materials considered for the components of the system must show resistance to corrosion and thermal fatigue caused by high temperature, oxidation and creep [38,39].

2.3. Heat transfer model

The heat transfer model is based on the law of conservation of energy. The model developed use several energy balances between the HTF and the surrounding environment (Fig. 4). These energy balances include all necessary equations and correlations to predict the terms of that balance, which depend on both the environmental conditions and the type and working conditions of the receiver. A literature review on the receiver models, shows that short length collector's ($L < 100$ m) gives good results with a 1-D energy balance, while for long length collector, a 2-D model is necessary [16]. The 1-D heat transfer model is the most often used approach in the literature compared to the multi-dimensional models, especially since it involves less power demand and complexity. Therefore, in this work a 1-D model is used in order to predict the PTC performance, and to reduce computational costs.

The heat transfer process is summarized as follows. The incident

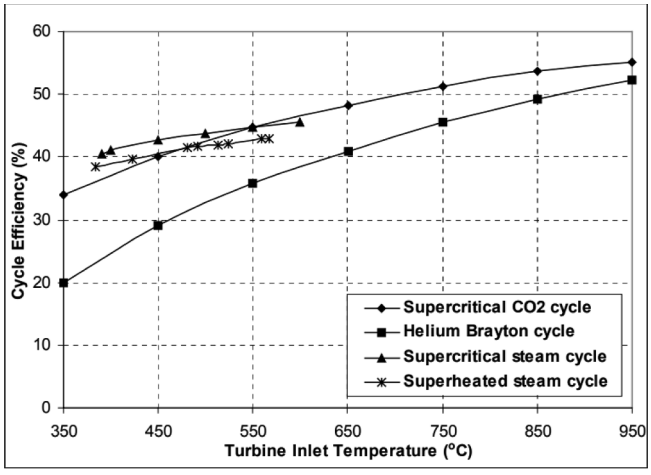

Fig. 3. Cycle efficiency comparison of thermal power cycles at temperatures relevant for CSP systems [37].

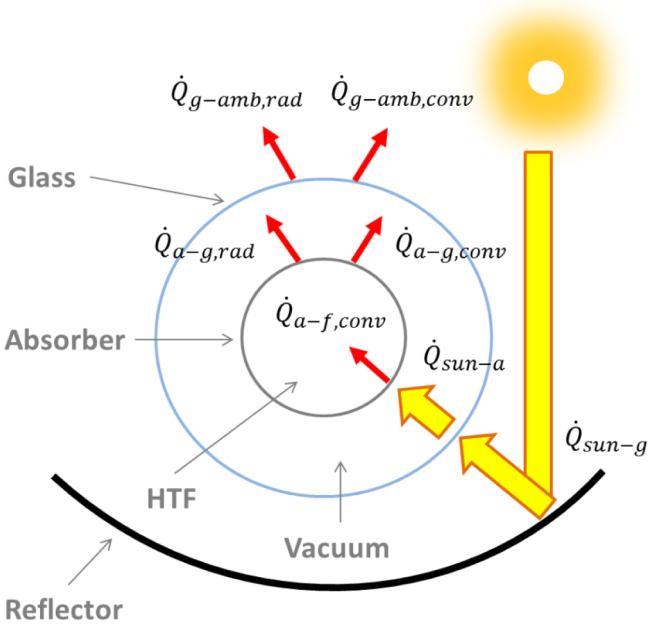

Fig. 4. Schematic diagram of the cross section of a parabolic-trough with one-dimensional steady-state energy balance.

solar energy onto the receiver tube is absorbed by the glass envelope ($\dot{Q}_{sun-g}$) and absorber tube ($\dot{Q}_{sun-a}$). Part of the incoming energy is transferred through the absorber tube to the HTF by convection ($\dot{Q}_{a-f,conv}$). The remaining energy is returned to the glass envelope by convection ($\dot{Q}_{a-g,conv}$) and radiation ($\dot{Q}_{a-g,rad}$). This energy transmitted back is lost through the glass envelope to the environment by convection ($\dot{Q}_{g-amb,conv}$) and radiation ($\dot{Q}_{g-amb,rad}$).

2.4. Assumptions

The energy-balances adopted in this work have been formulated based on the following assumptions:

- Steady-state condition.
- Incident radiation is treated as heat flux terms.
- Temperatures, heat flux and thermodynamic properties are uniform around the circumference in the cross section of the absorber.
- Based on Reynolds number, turbulent flow is considered.
- Vacuum is perfectly maintained between glass cover and absorber tube.
- Heat losses through support brackets are neglected.
- Heat conduction between the inner and outer surface of absorber and glass are neglected.
- Pressure losses are neglected.
- Natural convection from the glass envelope to the environment (no wind case).

2.5. Energy governing equations

Three control volumes are considered for 1-D model in this work: glass cover (g), absorber tube (a), heat transfer fluid (f); generating three interfaces: fluid-absorber ($f-a$), absorber-glass ($a-g$), glass-ambient ($g-amb$). The equations obtained for each interface are described as follow:

2.5.1. Fluid-absorber interface:

The solar radiation received by the absorber tube is transferred to the working fluid that flows through the absorber transforming the solar radiation into convective heat. The variation in the fluid temperature is:

$$Q_{a-f,conv} = h_f \cdot A_a \cdot (T_a - T_f) = \dot{m}_f \cdot c_{p,f} \cdot \Delta T_f \tag{1}$$

The outer absorber area A_a is calculated using a differential of length according to Eq. (2), so that it is possible to obtain temperature values at each point along to the absorber.

$$A_a = \pi \cdot D_{a,o} \cdot dl \tag{2}$$

where $D_{a,o}$ is the outer diameter of the absorber tube. The differential length is calculated as the ratio of the total length of the receiver L to the number of nodes N considered.

$$dl = \frac{L}{N} \tag{3}$$

2.5.2. Absorber-glass interface

The equation that determines the energy balance in the second interface is shown in Eq. (4).

$$\dot{Q}_{sun-a} = \dot{Q}_{a-f,conv} + \dot{Q}_{a-g,conv} + \dot{Q}_{a-g,rad} \tag{4}$$

2.5.3. Glass-ambient interface

The energy balance in this interface is given by the following equation:

$$\dot{Q}_{sun-g} + \dot{Q}_{a-g,conv} + \dot{Q}_{a-g,rad} = \dot{Q}_{g-amb,conv} + \dot{Q}_{g-amb,rad} \tag{5}$$

2.6. Heat flux terms

Each terms in the energy balance Eqs. (1), (4), and (5) are discussed below [16,40].

2.6.1. Incident solar radiation:

Incident solar radiation absorbed by the linear receiver in the glass envelope and the absorber tube are determined by the following expressions:

$$\dot{Q}_{sun-a} = G_b \cdot \cos(\theta) \cdot \eta_{opt,0^\circ} \cdot K(\theta) \cdot w \cdot dl \tag{6}$$

$$\dot{Q}_{sun-g} = G_b \cdot \cos(\theta) \cdot \alpha_g \cdot r \cdot \gamma_T \cdot K(\theta) \cdot w \cdot dl \tag{7}$$

where $\eta_{opt,0^\circ}$ is the nominal optical efficiency given by the Eq. (8) [41], γ_T is the overall intercept factor given by the Eq. (9) and $K(\theta)$ is the Incidence Angle Modifier (IAM) [41].

$$\eta_{opt,0^\circ} = r \cdot \tau_g \cdot \alpha_a \cdot \gamma_T \tag{8}$$

$$\gamma_T = \gamma_R \cdot \gamma_C \tag{9}$$

2.6.2. Convection heat transfer absorber-fluid

According to Newton's law of cooling, the convection heat transfer from the absorber to the HTF is given by the following equation:

$$\dot{Q}_{a-f,conv} = h_f \cdot \pi \cdot D_{a,i} \cdot dl \cdot (T_a - T_f) \tag{10}$$

where h_f is the convection heat transfer coefficient for the fluid that is calculated by the Eq. (11):

$$h_f = Nu_f \cdot \frac{k_f}{D_a} \tag{11}$$

For turbulent and transitional flow in tubes the following Nusselt number correlation developed by Petukhov [42] is used:

$$Nu_f = \frac{(f_2/8) \cdot \mathrm{Re} \cdot \mathrm{Pr}_f}{1.07 + 12.7 \cdot \sqrt{f_2/8} \cdot (\mathrm{Pr}_f^{2/3} - 1)} \tag{12}$$

According to Petukhov's results, Eq. (12) can predict experimental results with an accuracy of 1% within a range of $10^4 < \mathrm{Re} < 5 \cdot 10^6$ and $0.5 < \mathrm{Pr} < 20000$ [21], where Re and Pr are the Reynolds number and

the Prandtl number respectively, and f_2 is the Darcy friction factor [43].

2.6.3. Convection heat transfer absorber-glass

Considering vacuum in the space between the absorber and the glass envelope (pressure < ~1 torr), the convection heat transfer between the absorber and glass envelope occurs by free-molecular convection.

$$\dot{Q}_{a-g,conv} = h_v \cdot \pi \cdot D_{a,o} \cdot dl \cdot (T_a - T_g) \tag{14}$$

where h_v is the convection heat transfer coefficient for the vacuum [16], calculated by the Eq. (15).

$$h_v = \frac{k_{vacuum}}{\left(D_{a,o} \Big/ \left(2 \cdot \ln\left(\frac{D_{g,i}}{D_{a,o}} \right) \right) + b \cdot \lambda \cdot \left(\frac{D_{a,o}}{D_{g,i}} + 1 \right) \right)} \tag{15}$$

Being $k_{vacuum} = 0.02551(\mathrm{W/(m \cdot K)})$ the thermal conductance of the vacuum at standard temperature and pressure, $b = 1.571$ the interaction coefficient and $\lambda = 0.8867(\mathrm{m})$ the mean-free-path between collisions of a molecule [16].

2.6.4. Radiation heat transfer absorber-glass

The radiation heat transfer between the absorber tube and the glass envelope is estimated with the following equation:

$$\dot{Q}_{a-g,rad} = \frac{\sigma \cdot \pi \cdot D_{a,o} \cdot dl \cdot (T_a^4 - T_g^4)}{\left(\frac{1}{\varepsilon_a} + \frac{(1-\varepsilon_g) \cdot D_{a,o}}{\varepsilon_g \cdot D_{g,i}} \right)} \tag{16}$$

2.6.5. Convection heat transfer glass-ambient

The convection heat transfer from the glass envelope to the ambient is the largest source of heat loss. From Newton's law of cooling:

$$\dot{Q}_{g-amb,conv} = h_{air} \cdot \pi \cdot D_{g,o} \cdot dl \cdot (T_g - T_{amb}) \tag{17}$$

In the theoretical absence of wind, the convection heat transfer from the glass envelope to the environment will take place by natural convection. The correlation used to estimate the Nusselt number is the Churchill and Chu correlation [44]

$$Nu_{air} = \left(0.60 + \frac{0.387 \cdot Ra^{1/6}}{(1 + (0.559/\mathrm{Pr}_{g-amb})^{9/16})^{8/27}} \right)^2 \tag{18}$$

where Pr_{g-amb} is the Prandtl number evaluated at $(T_g + T_{amb})/2$.

2.6.6. Radiation heat transfer glass-ambient

The radiation heat transfer occurs because of the temperature difference between the glass envelope and sky. To approximate radiation loss, the envelope is assumed to be a small convex gray object in a large blackbody cavity.

$$\dot{Q}_{g-amb,rad} = \sigma \cdot \varepsilon_g \cdot \pi \cdot D_{g,o} \cdot dl \cdot (T_a^4 - T_{sky}^4) \tag{20}$$

where T_{sky} is the effective sky temperature(K)[21], related to the ambient temperature as follows the Eq. (21):

$$T_{sky} = 0.0553 \cdot (T_{amb})^{1.5} \tag{21}$$

2.7. Boundary conditions

The boundary conditions that determine the performance of the system are introduced as input parameters in the model. The main inputs parameters are: direct solar irradiance (G_b), angle of incidence to the beam solar radiation (θ), mass flow rate for the HTF ($\dot{m}_f$), ambient temperature close to the collector (T_{amb}), inlet temperature of the HTF inside the collector (T_f^i). Moreover, the inlet temperature of absorber tube (T_a^i) and inlet temperature of the glass envelope (T_g^i) are used for initialization. The values adopted are presented in Eq. (22) and Eq. (23) respectively based on experience. These values have no influence on the final results of the model as they are recalculated and updated automatically in model.

$$T_a^i = T_f^i + 20\ \mathrm{K} \tag{22}$$

$$T_g^i = 343\ K \tag{23}$$

When all the calculations are made, the model returns the following parameters as outputs: HTF outlet temperature (T_f^o), absorber tube outlet temperature (T_a^o) and glass envelope outlet temperature (T_g^o), convective heat transfer coefficient for the fluid (h_f), convective heat transfer coefficient to ambient (h_{air}) and convective heat transfer coefficient for the vacuum (h_v).

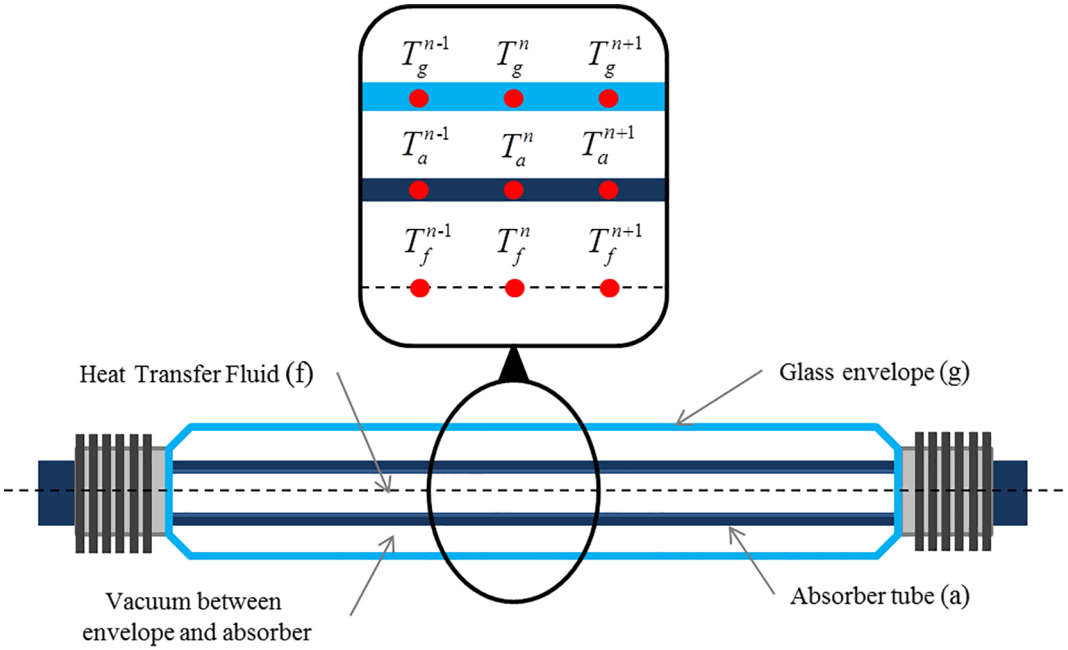

Fig. 5. Discretization domain along the receiver axis direction diagram.

2.8. Numerical procedure

Once obtained the equations that describe the system, the next step is to solve the system of three equations with three unknowns. To do this, the expressions showed previously are replaced into Eqs. (1), (4), and (5). Aiming to simplifying the expressions and facilitating the resolution of the system of equations proposed, the following constants are defined:

$$a = \dot{m}_f \cdot c_{p,f} \tag{24}$$

$$b = G_b \cdot \cos(\theta) \cdot \eta_{opt,0^\circ} \cdot K(\theta) \cdot w \cdot dl \tag{25}$$

$$c = h_f \cdot A_a \tag{26}$$

$$d = h_v \cdot A_a \tag{27}$$

$$e = \frac{\sigma \cdot A_a}{\left(\frac{1}{\varepsilon_a} + \frac{(1-\varepsilon_g)\cdot D_a}{\varepsilon_g \cdot D_g}\right)} \tag{28}$$

$$f = G_b \cdot \cos(\theta) \cdot \alpha_g \cdot r \cdot \gamma_T \cdot K(\theta) \cdot w \cdot dl \tag{29}$$

$$g = h_{air} \cdot A_g \tag{30}$$

$$h = \sigma \cdot \varepsilon_g \cdot A_g \tag{31}$$

Resulting the following system of equations:

$$c \cdot (T_a^n - T_f^n) - a \cdot (T_f^n - T_f^{n-1}) = 0 \tag{32}$$

$$b - c \cdot (T_a{}^n - T_f^n) - d \cdot (T_a^n - T_g^n) - e \cdot ((T_a^n)^4 - (T_g^n)^4) = 0 \tag{33}$$

$$f + d \cdot (T_a^n - T_g^n) + e \cdot ((T_a^n)^4 - (T_g^n)^4) - g \cdot (T_g^n - T_{amb}) - h \cdot ((T_g^n)^4 - (T_{sky})^4) = 0 \tag{34}$$

The next step is to discretize the domain of the system. Thus, the continuous domain of the problem under study is replaced by an homogeneous mesh. In the 1-D case studied here, the domain is divided by a discrete number of points, called nodes, where the numerical solution is calculated. This paper considers three 1-D and homogeneous meshes, one for each interface of the system under study: 1) Glass envelope, 2) Absorber tube, and 3) HTF. Fig. 5 shows a diagram of the mesh considered.

It is necessary to find T_f^n, T_a^n, T_g^n from the above Eqs. (32), (33), (34). As the equations of the system are fourth order magnitude, due to the Stefan-Boltzmann law, the Matlab function "ROOTS" is used to get the analytical solution of this system. The temperature at each point of the mesh considered can be obtained solving iteratively for every node.

2.9. Mesh independence study

The model discretizes the receiver into a finite number of control volumes along the length. Another relevant parameter in the model is the number of nodes considered in the mesh (space discretization). This parameter directly affects the accuracy of the numerical values obtained from simulations. Theoretically, if the number of nodes were too high, an accurate approximation is achieved. However, this leads to higher computational costs that make this possibility ruled out. To avoid this limitation and achieve a reasonable approximation in the simulation results, it is necessary to determine the optimal value of the number of nodes that must be considered.

The next methodology is used to get the optimum number of nodes:

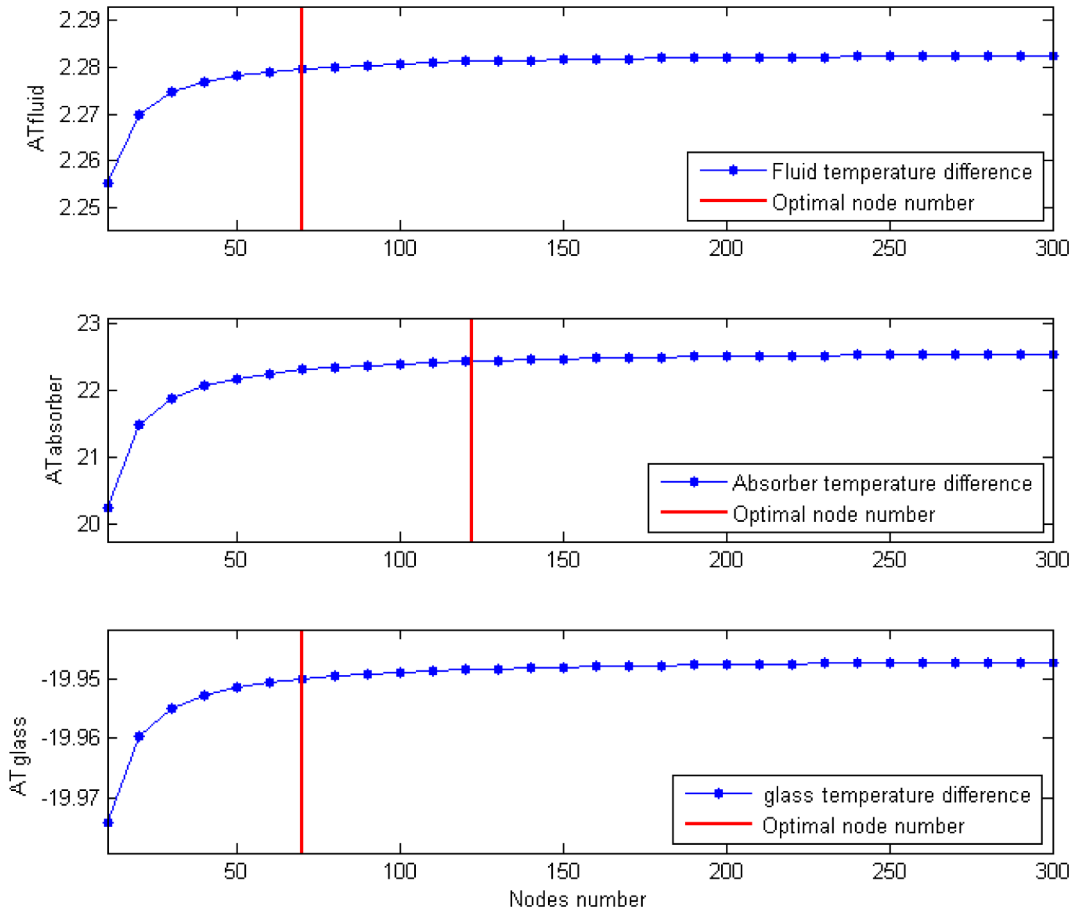

Fig. 6. Temperature differences of each model output's variable to determine the optimal number of nodes.

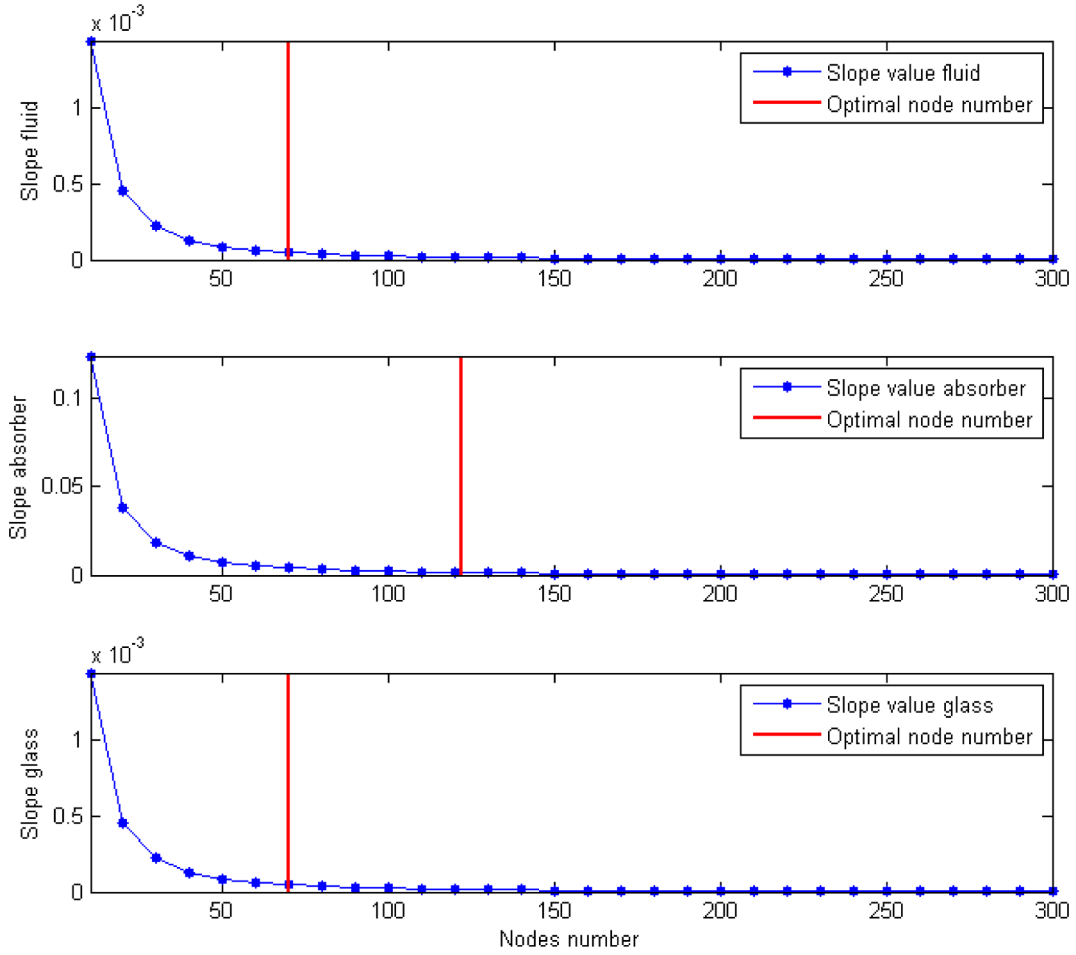

Fig. 7. Determination of the optimal number of nodes with slope of each model output's variable.

several simulations are performed keeping fixed conditions, and updating only the number of nodes. After each simulation, the temperature difference between input and output values is stored. This difference tends to converge as the number of nodes increases.

Figs. 6 and 7 present the temperature differences and the slopes of the curve as function of the number of nodes for each model output's variable. The most suitable number of nodes is reached when the variation in the slope is less than one thousandth, as it is the point where the slope of the curve reaches its minimum value. If higher value of nodes is considered, the numerical results of the simulation hardly suffer significant improvement.

This process is simultaneously carried out for the temperature difference in the fluid, absorber and glass envelope. So, it is possible that the number of nodes do not match for the three variables. To overcome this situation, the highest number of nodes is adopted. Thus, with this strategy, it is obtained accurate values regardless of the mesh considered in the domain. In the simulation presented in Figs. 6 and 7, the optimal number of nodes is 122.

3. Results and discussion

The most meaningful outputs among the responsible variables of the thermal behaviour of the PTC are the HTF outlet temperature and the thermal efficiency of the PTC. So, these variables are adopted for comparison between experiments and simulations. The deviation (D) between the results and the reference data considered is presented.

$$Deviation = \left(1 - \frac{Numerical}{Experimental}\right)\cdot 100 \tag{35}$$

where *Numerical* and *Experimental* represent the simulated and experimental values respectively.

Table 4
Comparison of numerical results with experimental data for Syltherm®800 with normal incidence.

Case	Input					Output					
						Experimental data [41]		Model data		Deviation	
	θ (°)	G_b (W/m^2)	HTF flow (m^3/h)	T_{amb} (K)	T_f^i (K)	T_f^o (K)	η_{th} (%)	T_f^o (K)	η_{th} (%)	D_T (%)	D_η (%)
1	0	815	15.01	304.4	377.8	416.1	70.3	418.9	75.5	0.7	7.5
2	0	910	14.90	304.1	379.1	422.7	71.0	426.6	77.5	0.9	9.1
3	0	877	14.11	305.8	378.4	420.6	67.5	423.5	72.2	0.7	7.0
4	0	918	14.99	308.8	379.6	422.4	69.6	426.0	75.5	0.9	8.6
5	0	981	15.06	309.3	386.2	432.8	71.1	435.6	75.5	0.6	6.2

Table 5
Comparison of numerical results with experimental data for Syltherm®800 for different incidence angles.

Case	Input					Output					
						Experimental data [41]		Model data		Deviation	
	θ (°)	G_b (W/m^2)	HTF flow (m^3/h)	T_{amb} (K)	T_f^i (K)	T_f^o (K)	η_{th} (%)	T_f^o (K)	η_{th} (%)	D_T (%)	D_η (%)
1	9.2	927	15.01	306.8	589.5	635.5	65.9	639.8	72.2	0.7	9.5
2	16.1	943	14.97	307.1	557.9	603.0	65.5	605.1	68.6	0.3	4.7
3	18.4	894	14.74	301.9	523.6	565.5	65.0	566.9	67.2	0.2	3.4
4	21.3	833	15.03	299.4	589.5	627.4	60.9	628.7	63.0	0.2	3.5
5	26.9	798	14.98	298.6	559.0	593.0	58.7	592.4	57.6	−0.1	−1.8

3.1. Synthetic oil

Syltherm®800 has been considered to verify the accuracy of the numerical model implemented, then the numerical results have been compared with experimental data obtained from tests carried out at the HTF test loop installed at PSA [41]. The detailed solar PTC specifications, presented in Table 1 and Table 3, are input parameters in the model. The thermal properties of the Syltherm®800 have been taken from [28].

The comparison of the performance between the numerical results and the experimental data are shown in Table 4 for normal incidence and Table 5 for different incidence angles, where T_f^i is the average HTF temperature at the inlet of the receiver and T_f^o is the HTF temperature at the outlet of the receiver. For the HTF outlet temperature in the 10 cases evaluated, 5 cases with normal incidence and 5 cases with different angles of incidence, it is shown:

- The maximum temperature deviation (D_T) obtained for normal incidence is 0.9%, with a mean deviation of 0.8%.
- The maximum temperature deviation (D_T) obtained for different incident angle is 0.7%, with a mean deviation of 0.3%.
- Maximum temperature deviations (D_T) correspond to cases #2 and #1 respectively, where the differences are of 4 K in both cases. The remaining cases show differences lower than 3 K.

Concerning the PTC thermal efficiency, the maximum deviation (D_η) remains below 10% for all the cases, which is an acceptable value for the quasi-steady state approach considered.

The results show that numerical HTF temperatures are slightly higher than the experiment data. It could be attributed to the simplifications adopted in the thermal model implemented (section 2.4), such as assuming no wind condition in thermal losses by convection from the glass to the environment, and neglecting the thermal losses through brackets of the receivers. So the thermal losses associated to the HCE may be slightly underestimated. It is translated into a greater contribution of energy on the HCE, what would explain the higher outlet temperature obtained in the simulation. Moreover, the discrepancies between the numerical results and the experimental measurements seem to decrease for higher incidence angles. This may be due to the fact that the optical and geometrical losses adopt a greater importance by considering incidence angles not null, shorting the difference between the results. With regard to the PTC thermal efficiency, the higher the temperature deviation is the higher the thermal efficiency deviation. A good degree of correlation has been obtained for quite different working conditions. So it can be concluded that despite the simplicity of the model, the numerical results are in reasonable good accordance with experimental ones, and the 1-D model is reliable to predict the thermal behaviour of PTC.

3.2. Carbon dioxide – Subcritical conditions

Pressurized carbon dioxide at subcritical conditions is simulated as HTF in this section. Subcritical conditions mean that the carbon dioxide flows through the solar receiver at a pressure and temperature below the critical point (Fig. 2). The numerical results from simulations have been verified with operation data obtained from a tests campaign performed in the pressurised gas test loop at PSA (Fig. 1) [30]. The PTC geometrical and optical input parameters used are presented in Tables 2 and 3.

Table 6 present the results for 6 cases where the maximum and mean deviations for the temperature (D_T) are 2.9% and 1.4% and for the thermal efficiency (D_η) are 14.7% and 7.4% respectively. Once more it is seen that for small incidence angle ($\theta = 3°$), greater discrepancies are shown. The maximum deviations corresponds to cases #1 and #2, with an incident angle of 3°, where the differences in temperature are of 17 and 14 K respectively. Most of the cases studied have differences lower than 8 K between numerical and experimental results.

Previously Serrano et al. [21] developed a thermal model using steam as HTF in a PTC. Contrasting the results and the measurements taken in a DSG solar test facility located at PSA, the maximum deviation for the temperature (D_T) obtained was 0.2% with a mean deviation of 0.1% and for the thermal efficiency (D_η) were 18% and 10% respectively. Even though, the HTF and the total length of the receiver studied

Table 6
Comparison of model predictions with experimental results for subcritical carbon dioxide. For all the cases showed in the table $T_{amb} = 303$K .

Case	Input					Output					
						Experimental data [30]		Model data		Deviation	
	θ (°)	θ (MPa)	G_b (W/m^2)	$\dot{m}_f$ (kg/s)	T_f^i (K)	T_f^o (K)	η_{th} (%)	T_f^o (K)	η_{th} (%)	D_T (%)	D_η (%)
1	3.0	6.5	957	1.33	459.0	574.6	63.6	591.4	72.9	2.9	14.7
2	3.0	6.5	941	1.33	568.8	673.0	59.5	686.6	67.4	2.0	13.3
3	11.0	6.5	924	1.25	453.0	575.9	65.8	580.4	68.2	0.8	3.7
4	11.0	6.5	924	1.25	565.1	673.0	59.0	679.7	62.7	1.0	6.3
5	17.2	6.5	670	0.82	560.4	672.5	55.4	672.0	55.1	−0.1	−0.5
6	17.2	6.5	677	0.82	445.6	581.5	65.2	573.7	61.4	−1.3	−5.8

in present model are not the same, it is reasonable to think that numerical results for carbon dioxide at subcritical conditions have a good agreement with measurements.

3.3. Carbon dioxide – Supercritical conditions

The last HTF simulated is carbon dioxide at supercritical (sCO_2) conditions. Unfortunately, there is lack of experimental information to check the numerical results. However, previous works simulated the performance of sCO_2 as working fluid, and those results are used for comparison. Muñoz-Antón et al. [29] analysed the feasibility of using PTC cooled by gas at high pressures and temperatures. The simulated facility in Muñoz-Antón's work is the same as described in the section 3.2 for subcritical carbon dioxide, so the same geometrical and optical parameters are used.

Table 7
Comparison of model predictions with Muñoz-Antón's results for supercritical carbon dioxide. For all the cases showed in the table $T_{amb} = 303K$.

Case	Input					Output					
						Experimental data [29]		Model data		Deviation	
	θ (°)	θ (MPa)	G_b (W/m^2)	$\dot{m}_f$ (kg/s)	T_f^i (K)	T_f^o (K)	η_{th} (%)	T_f^o (K)	η_{th} (%)	D_T (%)	D_η (%)
1	0	7.5	900	0.94	498	798	64.2	819.3	68.9	2.7	7.4
2	0	7.5	900	1.32	498	723	67.0	727.7	68.4	0.7	2.1
3	0	10	900	0.93	498	798	64.8	819.6	69.6	2.7	7.4
4	0	10	900	1.30	498	723	67.5	728.1	69.0	0.7	2.3

Table 7 compares the numerical results of [29] with the numerical results of the model presented in this work for 2 different values of operation pressure (7.5, 10 MPa). It is noted from the results that the model generates greater deviations for low values of HTF inlet flow rate whatever the operating pressure. Low values in the HTF's input flow translate into a higher temperature of the fluid in the receiver, which subsequently means higher thermal losses. As previously was pointed out (Section 3.1), the present model underestimates the thermal losses leading to a greater deviation in the predictions of the HTF outlet temperature. As a consequence, cases #1 and #3 present higher deviations with temperature differences of 21 K and 22 K respectively. This comparison shows that model gives truthful results for sCO_2 state as working fluid, expecting small deviations. Overall, for the cases evaluated with sCO_2, the maximum temperature deviation is 2.7% with a mean deviation of 1.7%, while the maximum thermal efficiency deviation is 7.4%.

3.4. Sensitivity analysis

The aim of the sensitivity analysis performed in this work is to study relationships between model output and model input values, identifying which input parameters have a higher influence on the system performance.

The simplest method to carry out a sensitivity analysis is the one-at-a-time (OAT) method. This technique consists of modifying only the value of one input parameter at a time, while holding all other parameters fixed, and see how it affects the result of the analysis. This type of analysis is also called as local analysis, since it only studies the sensitivity in relation to the point estimates chosen and not for the complete parameter distribution [45]. The OAT method is performed over three input magnitudes: direct solar irradiance, fluid flow rate and fluid inlet temperature. These input parameters are varied around the gas-cooled trough-collector facility nominal conditions with carbon dioxide [30]. The values considered for the analysis are listed in the table 8.

The numerical results obtained from the sensitivity analysis are graphed for the following magnitudes: HTF temperature increase, thermal losses (convection and radiation) to the environment, heat convection coefficient of the HTF and the difference temperature between HTF and absorber wall at the outlet. In each figure, three graphs are drawn, one for each value of direct solar irradiance evaluated.

The increase in temperature experienced by the HTF in the collector and temperature difference between fluid and absorber tube at receiver end are plotted in Figs. 8 and 9 separately. It is seen that for each direct solar irradiance value adopted, the largest variation in these magnitudes' values is introduced by the fluid input flow rate while the fluid inlet temperature is hold. The highest differences in temperature are found for low input flow values in both figures. Moreover, holding the input flow the variation induced by the fluid inlet temperature is scarce. Though for a lower value of HTF input temperature, within the same mass flow value, the predictions obtained for these magnitudes are marginally higher. Finally, it is seen that the higher the direct solar irradiance, the higher these variations are in both figures.

Table 8
Values range considered for the sensitivity analysis of the parameters subjected to study.

Parameter	Value			Unit
G_b	700	850	1000	W/m^2
$\dot{m}_f$	0.9	1.36	1.59	kg/s
T_f^i	458	478	498	K

Fig. 10 presents the overall heat losses, by convection and radiation, from the HCE to environment. The same behaviour observed previously is repeated, and the most significant variation is introduced by the input mass flow rate, for the same value of direct solar irradiance and holding the HTF input temperature. Nevertheless, unlike Figs. 8 and 9, the variations in results induced by the fluid inlet temperature are visible in this case, so, as the HTF temperature increases, the heat losses to the environment are higher.

Finally, the heat transfer coefficient between absorber tube and fluid is shown in Fig. 11. Unlike the previous figures, the results show a different trend. This magnitude shows the same pattern for the three direct solar irradiance's values studied. Only the HTF inlet flow rate is the input parameter that causes the higher variation in the output. The heat transfer convection coefficient increases as the input mass flow rate increases. Liao et al. [46] study experimentally the effect of some important parameters, including mass flow rate and bulk fluid temperature in heat transfer coefficients from sCO_2 flowing in mini/micro circular tubes for several inside-diameters in the temperature ranges relevant to the CO_2 gas cooler. Although, different values of inside-diameters and mass flow rates from those considered in present work were tested, the heat transfer coefficient for carbon dioxide shows the same pattern of performance than the obtained in the sensitive analysis. The convective coefficient for a similar pressure of 100 bar, slightly decreases as bulk CO_2 temperature rises and increases for higher mass flow values.

The sensitivity analysis proves that the parameters that more

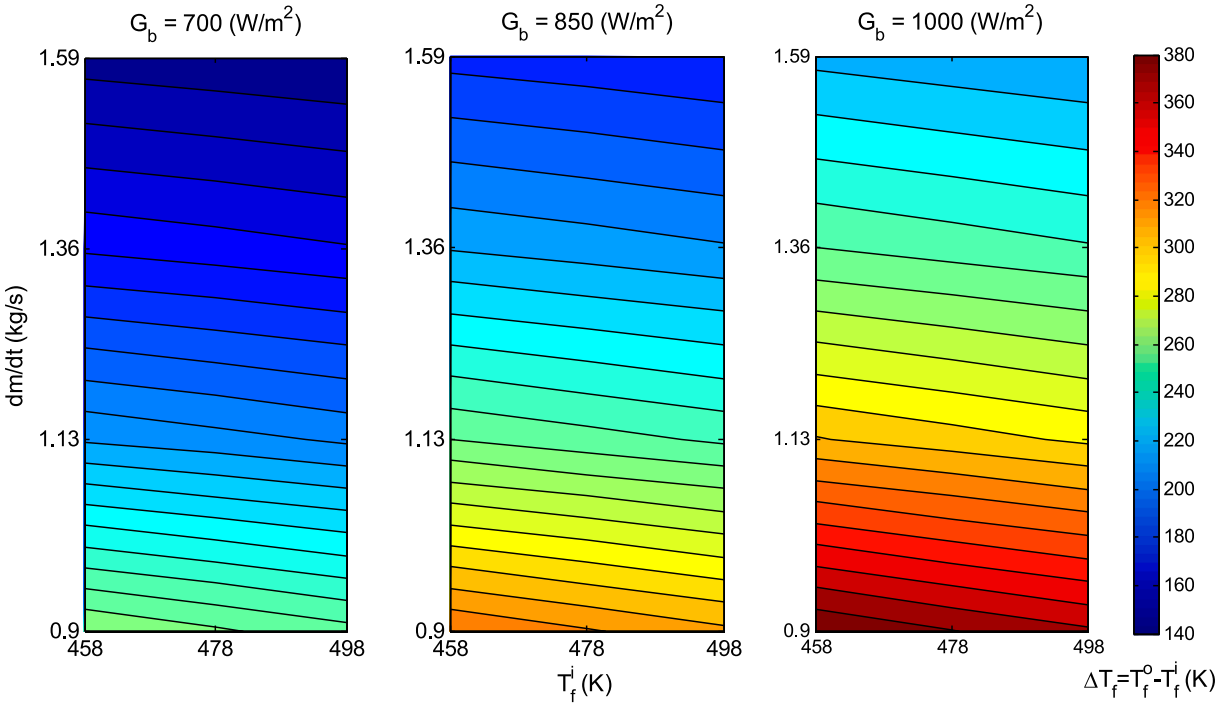

Fig. 8. HTF temperature increase as a function of inlet HTF mass flow and temperature, for three values of direct solar irradiance.

variation introduces in the results of the model are the direct solar irradiance and, for the same value of direct solar irradiance, the HTF inlet flow rate. Only the heat transfer coefficient seems to remain impassive to the different working conditions studied. In any case, the mass flow rates lead to higher variations in model outputs than HTF inlet temperatures. Only for the heat loss from the HCE to environment (Fig. 10) the variations induced by the HTF inlet temperature are significant.

4. Conclusions

This work presents a simplified one-dimensional thermal model to study the thermal behaviour of PTC using carbon dioxide at supercritical conditions as HTF. Its implementation has been performed from the basic governing equations, and has been written in Matlab®. A complete description of all the equations, parameters, and variables is

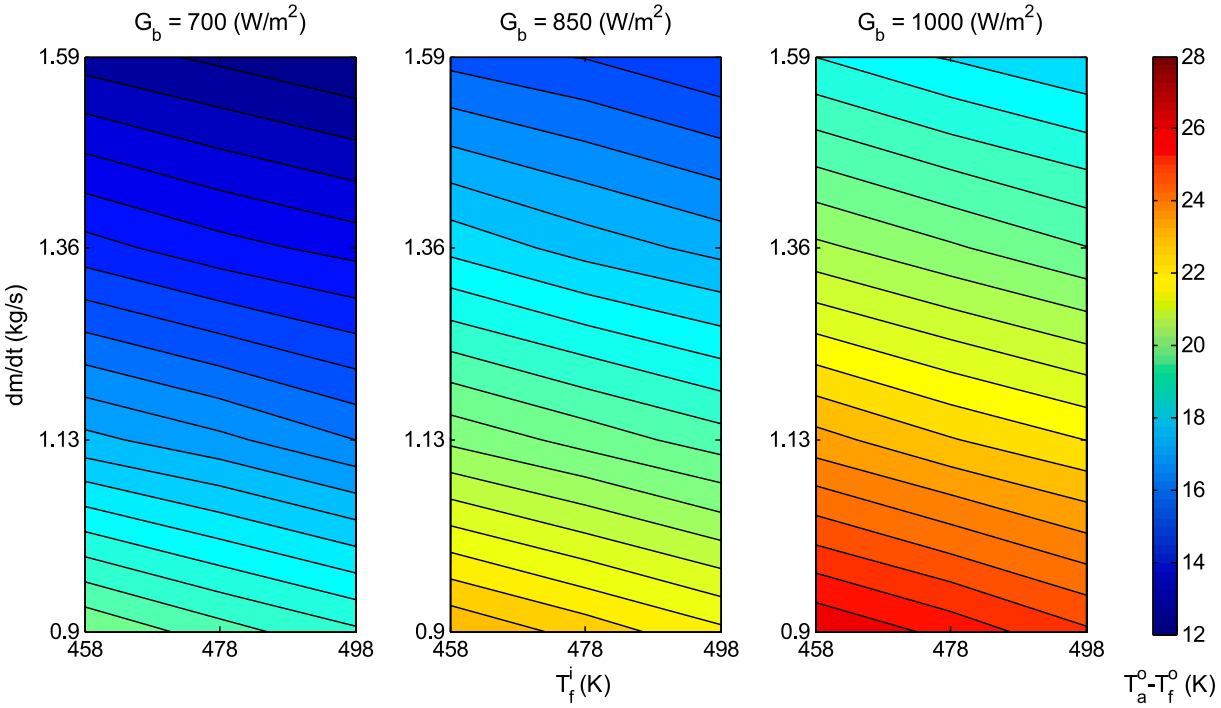

Fig. 9. Temperature difference between HTF and absorber tube at collector exit as a function of inlet HTF mass flow and temperature, for three direct solar irradiance.

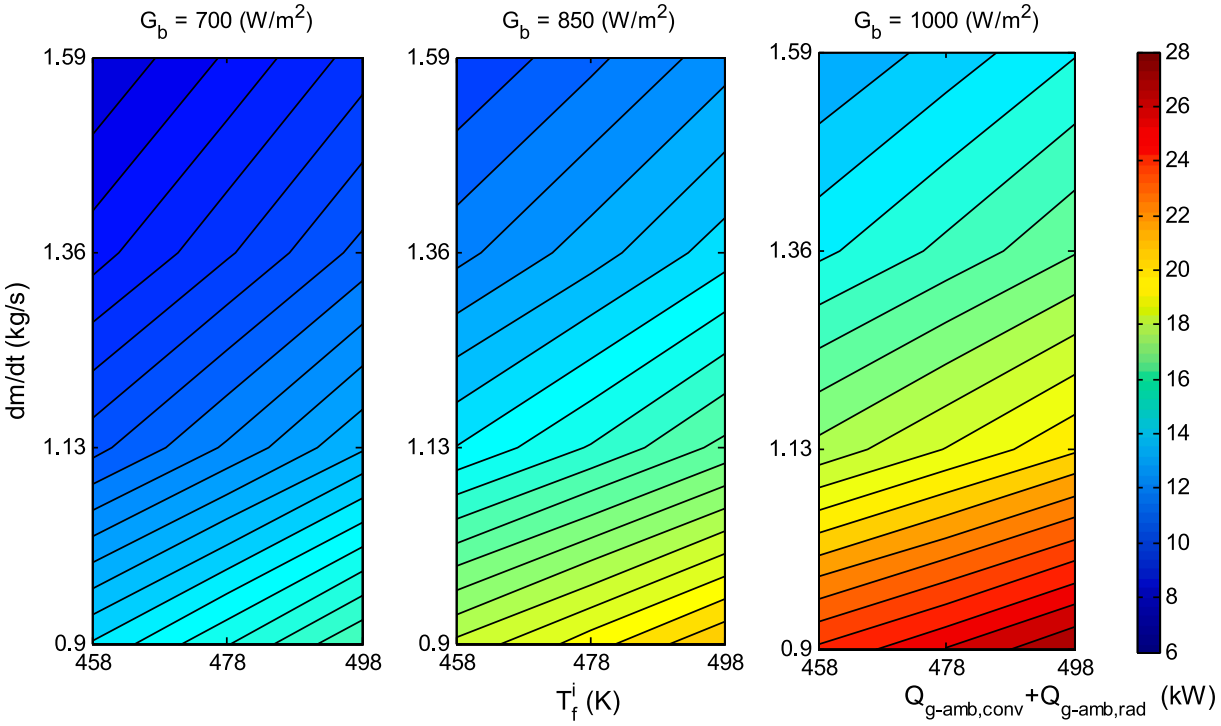

Fig. 10. Heat loss from the HCE to environment (convection + radiation) as a function of inlet HTF mass flow and temperature, for several direct solar irradiance values.

given. The methodology to perform a mesh independence study to get accurate approximations in the simulation results has been devised and incorporated into the model.

The proposed model has been examined using three different HTFs; thermal oil, CO_2 at subcritical and CO_2 at supercritical conditions. The HTF outlet temperature and the thermal efficiency are the parameters used for comparison. The predicted results were compared with experimental data for different operating conditions in thermal oil and subcritical carbon dioxide cases. The maximum deviations achieved in HTF outlet temperature are 0.9% and 2.9%, respectively. The good agreement between

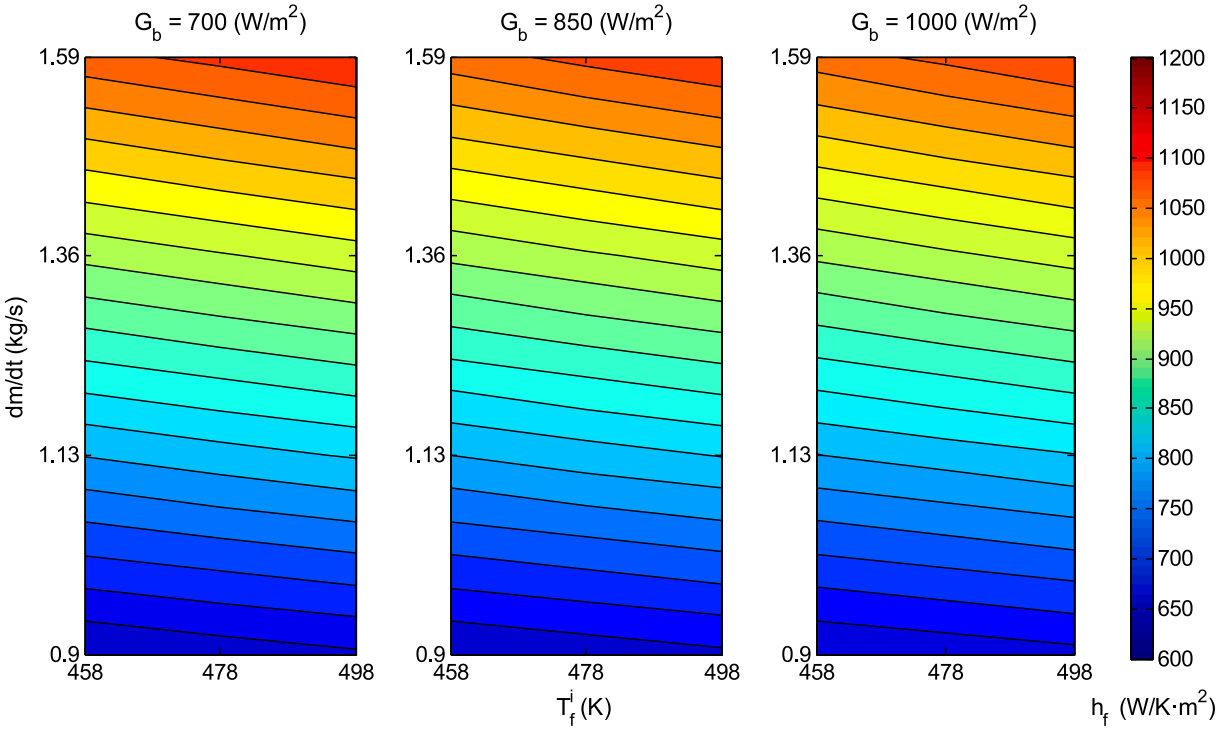

Fig. 11. The heat transfer coefficient between absorber and HTF as a function of inlet HTF mass flow and temperature, for several direct solar irradiance values.

experimental and numerical results shows that the 1-D model for the receiver tube is trustworthy. However, it has been observed that model has a slight deviation in the estimation of heat losses to the environment as consequence of the simplifications adopted.

After the model is compared with experimental data, it is further used to simulate the thermal behaviour of sCO_2 as working fluid in PTCs. The predictions are compared with literature results in order to determine its accuracy. The maximum temperature deviation of 2.7% is reported for results with sCO_2 with low value of HTF flow which is considered acceptable for a 1-D model with the assumptions considered. Finally, a sensitivity analysis was conducted by the one-at-a-time method on three input parameters: inlet HTF mass flow rate, inlet HTF temperature and direct solar irradiance. The increase in HTF temperature, temperature difference between HTF and absorber tube, heat loss from the HCE to environment and the heat transfer coefficient between absorber and HTF were plotted to check the results. The analysis revealed that the parameter that causes the greatest variations on the model outputs are the direct solar irradiance and, for a given value of this, the HTF inlet flow rate.

Declaration of Competing Interest

None.

Acknowledgements

The research work leading to this article has been developed under the framework of the DETECSOL project (ENE2014-56079-R), supported by the Spanish Department of Research, Development and Innovation. First author wishes to thank to CIEMAT for granting his Ph.D. research at Plataforma Solar de Almería.

References

[1] Abdulhamed AJ, Adam NM, Ab-Kadir MZA, Hairuddin AA. Review of solar parabolic-trough collector geometrical and thermalanalyses, performance, and applications. Renew Sust Energy Rev 2018;91:822–31. https://doi.org/10.1016/j.rser.2018.04.085.

[2] Manikandan GK, Iniyan S, Goic R. Enhancing the optical and thermal efficiency of a parabolic trough collector – a review. Appl Energy 2019;235:1524–40. https://doi.org/10.1016/j.apenergy.2018.11.048.

[3] Bellos E, Tzivanidis C. Alternative designs of parabolic trough solar collectors. Prog Energy Combust Sci 2019;71:81–117. https://doi.org/10.1016/j.pecs.2018.11.001.

[4] Baharoon DA, Rahman HA, Omar WZW, Fadhl SO. Historical development of concentrating solar power technologies to generate clean electricity efficiently – a review. Renew Sust Energy Rev 2015;41:996–1027. https://doi.org/10.1016/j.rser.2014.09.008.

[5] Ho CK. Advances in central receivers for concentrating solar applications. Sol Energy 2017;152:38–56. https://doi.org/10.1016/j.solener.2017.03.048.

[6] Vignarooban K, Xu X, Arvay A, Hsu K, Kannan AM. Heat transfer fluids for concentrating solar power systems – a review. Appl Energy 2015;156:383–96. https://doi.org/10.1016/j.apenergy.2015.01.125.

[7] Tian Y, Zhao CY. A review of solar collectors and thermal energy storage in solar thermal applications. Appl Energy 2013;104:538–53. https://doi.org/10.1016/j.apenergy.2012.11.051.

[8] Bellos E, Tzivanidis C, Antonopoulos KA, Daniil I. The use of gas working fluids in parabolic trough collectors – an energetic and exergetic analysis. Appl Therm Eng 2016;109:1–14. https://doi.org/10.1016/j.applthermaleng.2016.08.043.

[9] Benoit H, Spreafico L, Gauthier D, Flamant G. Review of heat transfer fluids in tube-receivers used in concentrating solar thermal systems: properties and heat transfer coefficients. Renew Sust Energy Rev 2016;55:298–315. https://doi.org/10.1016/j.rser.2015.10.059.

[10] Shakar J. Review and future trends of supercritical CO2 Rankine cycle for low-grade heat conversion. Renew Sustain Energy Rev 2015;48:434–51. https://doi.org/10.1016/j.rser.2015.04.039.

[11] Cheng WL, Huang WX, Nian YL. Global parameter optimization and criterion formula of supercritical carbon dioxide Brayton cycle with recompression. Energy Convers Manage 2017;150:669–77. https://doi.org/10.1016/j.enconman.2017.08.055.

[12] Silva-Pérez MA. Solar power towers using supercritical CO2 and supercritical steam cycles, and decoupled combined cycles. In: Blanco M, Ramirez Santigosa L, editors. Advances in Concentrating Solar Thermal Research and Technology. Woodhead Publishing; 2016. p. 383–402.

[13] Cabeza LF, de Gracia A, Fernández AI, Farid MM. Supercritical CO2 as heat transfer fluid: a review. Appl Therm Eng 2017;125:799–810. https://doi.org/10.1016/j.applthermaleng.2017.07.049.

[14] Muñoz-Antón J, Rubbia C, Rovira A. Martínez-Val JM. Performance study of solar power plants with CO_2 as working fluid. A promising design window. Energy Convers Manage 2015;92:36–46. https://doi.org/10.1016/j.enconman.2014.12.030.

[15] Manjunath K, Sharma OP, Tyagi SK, Kaushik SC. Thermodynamic analysis of a supercritical/transcritical CO_2 based waste heat recovery cycle for shipboard power and cooling applications. Energy Convers Manage 2018;155:262–75. https://doi.org/10.1016/j.enconman.2017.10.097.

[16] Forristall R. Heat transfer analysis and modeling of a parabolic trough solar receiver implemented in engineering equation solver. National Renewable Energy Laboratory; 2003:164. Technical report NREL/TP-550-34169.

[17] Dudley V, Kolb G, Sloan M, Kearney D. SEGS LS-2 solar collector-test results. Sandia Natl Lab 1994. SAN94-1884.

[18] Gong G, Huang X, Wang J, Hao M. An optimized model and test of the China's first high temperature parabolic trough solar receiver. Sol Energy 2010;84:2230–45. https://doi.org/10.1016/j.solener.2010.08.003.

[19] Padilla RV, Demirkaya G, Goswami DY, Stefanakos E, Rahman MM. Heat transfer analysis of parabolic trough solar receiver. Appl Energy 2011;88:5097–110. https://doi.org/10.1016/j.apenergy.2011.07.012.

[20] Kalogirou SA. A detailed thermal model of a parabolic trough collector receiver. Energy 2012;48:298–306. https://doi.org/10.1016/j.energy.2012.06.023.

[21] Serrano-Aguilera JJ, Valenzuela L, Parras L. Thermal 3D model for Direct Solar Steam Generation under superheated conditions. Appl Energy 2014;132:370–82. https://doi.org/10.1016/j.apenergy.2014.07.035.

[22] Qiu Y, Li MJ, He YL, Tao WQ. Thermal performance analysis of a parabolic trough solar collector using supercritical CO_2 as heat transfer fluid under non-uniform solar flux. Appl. Therm. Eng. 2017;115:1255–65. https://doi.org/10.1016/j.applthermaleng.2016.09.044.

[23] Kreith F, Pepper DW. Energy efficiency and renewable energy handbook. 2nd ed. Boca Raton: CRC Press; 2016.

[24] Geyer M, Osuna R, Esteban A, Schiel W, Schweitzer A, Zarza E, et al. EUROTROUGH–Parabolic trough collector developed for cost efficient solar power generation. 11th SolarPACES, Zurich: 2012, p. 1–7.

[25] Sallaberry F, Valenzuela L, Palacin LG. On-site parabolic trough collector testing in solar thermal power plants: experimental validation of a new approach developed for the IEC 62862–3-2 standard. Sol Energy 2017;155:398–409. https://doi.org/10.1016/j.solener.2017.06.045.

[26] SCHOTT PTR®70 Receivers Datasheet; 2013.

[27] Ma Z, Turchi CS. Advanced supercritical carbon dioxide power cycle configurations for use in concentrating solar power systems. National Renewable Energy Laboratories; 2011. Technical Report NREL/CP-5500-50787.

[28] Dow. SYLTHERM 800. Silicone heat transfer fluid. Product Information; 2001.

[29] Muñoz-Antón J, Biencinto M, Zarza E, Diez LE. Theoretical basis and experimental facility for parabolic trough collectors at high temperature using gas as heat transfer fluid. Appl Energy 2014;135:373–81. https://doi.org/10.1016/j.apenergy.2014.08.099.

[30] Rodriguez-Garcia M, Marquez-Payes JM, Biencinto M, Adler JP, Diez LE. First experimental results of a solar PTC facility using gas as the heat transfer fluid. 15th SolarPACES, Berlin; 2009, p. 1–8.

[31] Turchi CS. Supercritical CO2 for Application in Concentrating Solar Power Systems. SCCO2 Power Cycle Symposium, Troy; 2009 ,p.1–5.

[32] Persichilli M, Kacludis A, Zdankiewicz E, Held T. Supercritical CO2 Power Cycle Developments and Commercialization: Why sCO2 can Displace Steam. Power-Gen India & Central Asia, New Delhi: 2012, p.1–16.

[33] Weinstein LA, Loomis J, Bhatia B, Bierman DM, Wang EN, Chen G. Concentrating solar power. Chem Rev 2015;115(23):12797–838. https://doi.org/10.1021/acs.chemrev.5b00397.

[34] Muñoz J, Zarza E, Díez LE, Martínez-Val JM, López C, Gavela R, et al. The New Technology of Gas-Cooled Trough Collectors. International Symposium SolarPACES 2011, Granada, Spain, September 21-24, 2011.

[35] Cipollone R, Cinocca A, Gualtieri A. Gases as working fluid in parabolic trough CSP plants. Procedia Comput Sci 2013;19:702–11. https://doi.org/10.1016/j.procs.2013.06.093.

[36] Lemmon EW, McLinden MO, Friend DG. Thermophysical Properties of Fluid Systems. NIST Chemistry WebBook, NIST Standard Reference Database Number 69. In: P.J. Linstrom, W.G. Mallard (Eds.), National Institute of Standards and Technology, Gaithersburg MD, 20899. doi: 10.18434/T4D303.

[37] Dostal V. A Supercritical Carbon Dioxide Cycle for Next Generation Nuclear Reactors. Massachusetts Institue of Technology PhD Thesis Dept of Nuclear Engineering; 2004.

[38] Fleming DD, Pasch JJ, Conboy TM, Carlson MD, Kruzienga AM. Corrosion and Erosion Behavior in Supercritical CO2 Power Cycles. Sandia National Laboratories; 2014. Technical Report SAND2014-0602C.

[39] Liang Z, Wang Gui Y. Y Zhao Q. Corrosion performance of heat-resisting steels and alloys insupercritical carbon dioxide at 650 °C and 15 MPa. Energy 2019;175:345–52. https://doi.org/10.1016/j.energy.2019.03.014.

[40] Burkholder F, Kutscher C. Heat Loss Testing of Schott's 2008 PTR70 Parabolic Trough Receiver. Tech rep NREL/TP-550- 45633. National Renewable Energy Laboratory; 2009.

[41] Valenzuela L, Lopez-Martin R, Zarza E. Optical and thermal performance of large-size parabolic trough solar collectors from outdoor experiments: a test method and a case study. Energy 2014;70:456–64. https://doi.org/10.1016/j.energy.2014.04.016.

[42] Petukhov B. Heat transfer and friction in turbulent pipe flow with variable physical properties. Adv Heat Transfer 1970;6:503–64. https://doi.org/10.1016/S0065-

2717(08)70153-9.
[43] Goudar C, Sonnard J. Comparison of the iterative approximations of the Colebrook-White equation. Hydrocarbon Proc 2008;87(8):79–83.
[44] Churchill SW, Chu HHS. Correlating equations for laminar and turbulent free convection from a horizontal cylinder. Int J Heat Mass Transfer 1975;18(9):1049–53. https://doi.org/10.1016/0017-9310(75)90222-7.
[45] Pianosi F, Beven K, Freer J, Hall JW, Rougier J. Stephenson e DB, Wagener T. Sensitivity analysis of environmental models: a systematic review with practical workflow. Environ Modell Software 2016;79:214–32. https://doi.org/10.1016/j.envsoft.2016.02.008.
[46] Liao SM, Zhao TS. Measurements of heat transfer coefficients from supercritical carbon dioxide flowing in horizontal mini/micro channels. J Heat Transfer 2002;124(3):413–20. https://doi.org/10.1115/1.1423906.